JOURNAL OF MATERIALS SCIENCE 18 (1983) 257–264

Thermodynamic assessment of heat treatments for a Co–Cr–Mo alloy

KRISHNA RAJAN
National Aeronautical Establishment, National Research Council, Ottawa, Ontario, K1A 0R6, Canada

Ternary phase diagrams of the Co–Cr–Mo system have been calculated from thermodynamic data. It is shown that from such diagrams, intermetallic phase formation which is detrimental to mechanical behaviour, may be predicted. These calculations may be used to provide a thermodynamic basis for surgical implant alloy design.

1. Introduction

The Co–Cr–Mo alloy system is widely used as surgical implant material. It has been suggested that improvements in mechanical properties may be brought about by heat treatments [1]. The proper choice of an optimum heat treatment, however, requires a knowledge of the phase diagram for the alloy system under consideration. To experimentally generate a phase diagram for such a complex alloy as that used for surgical implants, however, is difficult. The purpose of this paper is to demonstrate the feasibility of calculating ternary phase diagrams at different temperatures for the Co–Cr–Mo system. The thermodynamic basis of the calculations is first reviewed and some typical results are given. The implications of these results in terms of the choice of heat treatments of cobalt-based surgical implant alloys is discussed. Finally the role of carbon in the Co–Cr–Mo system is examined.

2. Thermodynamics of phase-diagram calculations

Calculations were carried out using a package of computer programs developed by ManLabs, Inc.* The development of computer-based methods for phase-diagram calculations was due largely to Kaufman [2, 3]. The basis of these methods is the explicit definition of the free energy of solution and compound phases in metallic systems in terms of lattice stability, solution and compound parameters. These formulations provide explicit mathematical descriptions of the excess free energies of all the solution phases in the binary system.

The model employed in these programs assumes the form of the free energy of a solution phase, ϕ, in the binary system A–B to be:

$$G^{\phi} = x_A G_A^{\phi} + x_B G_B^{\phi} + \\ + RT(x_A \ln x_A + x_B \ln x_B) + G_E^{\phi}, \quad (1)$$

where G_I^{ϕ} is the free energy of pure I in the ϕ state, x_I is the mole fraction of phase I and the excess free energy is given by:

$$G_E^{\phi} = x_A x_B [x_A \alpha^{\phi}(T) + x_B \beta^{\phi}(T)] \quad (2)$$

The interaction parameters, α and β, are functions of absolute temperature given by:

$$\alpha = \alpha_0 + \alpha_1 T \quad (3)$$

$$\beta = \beta_0 + \beta_1 T. \quad (4)$$

(The programs can also handle T^2 and T^3 terms in the interaction parameters; these terms are useful near 0 K).

This model reduces to the regular solution model when $\alpha_0 = \beta_0 = \Omega$; $\alpha_1 = \beta_1 = 0$. It effectively allows Ω to be a linear function of composition. The first-order temperature dependence (α_1 and β_1) corresponds to an entropy term in the bound energies of the quasichemical model, which is also allowed to vary linearly with composition. Phase boundaries are calculated by determining, at a given temperature, T, where the chemical poten-

*ManLabs, Inc., 21 Erie Street, Cambridge, Mass. 02139, USA.

0022–2461/83/010257–08$03.46/0 © *1983 Chapman and Hall Ltd.*

tials of each species are equal in a pair of phases,

$$\mu_i = \frac{\partial G}{\partial x_i}_{T,P,x_j}$$

where P is the pressure and x_j is the mole fraction of species j.

The ManLabs programs are designed primarily for interactions between elements. They can also be found for compounds, provided that the edges A and B can be defined so that their ideal entropy of mixing is given by:

$$S^M = -R(x_A \ln x_A + x_B \ln x_B), \quad (5)$$

which is the form assumed by the programs.

The free energy of a ternary solution phase is defined in a similar manner:

$$G = x_A G_A + x_B G_B + x_C G_C + RT(x_A \ln x_A + x_B \ln x_B + x_C \ln x_C) + G_E, \quad (6)$$

where the excess free energy, G_E, is given by:

$$G_E = \frac{x_A x_B}{x_A + x_B}[x_A \alpha(T) + x_B \beta(T)] + \frac{x_A x_C}{x_A + x_C}[x_A \alpha(T) + x_C \gamma(T)] + \frac{x_B x_C}{x_B + x_C}[x_B \beta'(T) + x_C \gamma'(T)] + x_A x_B x_C \Delta(\text{comp}, T), \quad (7)$$

where α and β are the A–B binary interaction parameters, α' and γ' correspond to A–C, and β and γ' to B–C. All are linear in T, as before.

The ternary interaction parameter, Δ, is assumed to be zero throughout the present calculations. Therefore, the ternary phase diagram is determined if the binary interaction coefficients are specified. Consequently, the accuracy of the ternary phase diagram depends upon the accuracy of the calculated binary diagrams. Fortunately, there is enough experimental data for the Co–Cr, Co–Mo and Mo–Cr systems to provide explicit mathematical descriptions for the excess free energy expressions.

Some of the general features of the calculated phase diagrams will first be presented followed by the metallography of samples given the heat treatments at the calculated ternary isotherms. The relationship between the two will then be discussed, particularly in terms of σ-phase formation.

3. Results

3.1. Calculated phase diagrams

The Co–Cr binary (Fig. 1) as calculated does not show all the congruent intermetallic compounds at lower temperatures. However, at higher temperatures the comparison is more favourable. The highest calculated eutectic is at 1720 K while the experimental one is at ~1700 K. σ-phase formation is indicated as a peritectoid reaction by calculation while the experimental diagram shows it as a congruent transformation. In both cases, however, the temperature of the transformation is similar (1520 K – calculated, and ~1580 K – experimental).

For the Co–Mo system, the calculated and experimental eutectics are almost identical (1600 and 1605 K, respectively). The formation of the σ-phase in both cases is shown to be a peritectoid reaction. However, the temperature range for σ-phase stability is calculated to be from 1350 to 1790 K while the observed range is from 1523 to 1893 K.

The Mo–Cr system is the simplest binary, with a liquidus minimum and a solid miscibility gap in both calculated and observed phase diagrams. The calculated liquidus minimum is ~2180 K while the observed is at ~2080 K. The maximum in the solid miscibility gap is calculated to be ~1200 K while the observed maximum is close to that at ~1150 K. Overall, the observed and calculated phase diagrams as shown in Figs 1 to 3 compare favourably [4, 5].

For the purposes of the present study, the ternary phase diagram was calculated primarily in the composition range of the orthopaedic implant alloy as given by ASTM Specification F75-67 (Table I). With the Co–Cr binary, the interactions of interest are: $\sigma(Co_{0.4}Cr_{0.6})$-fcc, σ-hcp and fcc–hcp. From the Co–Mo system, the relevant interactions are: fcc–hcp, $\mu(Co_{0.538}Mo_{0.462}=Co_7Mo_6)$–fcc, $\kappa(Co_{0.75}Mo_{0.25}=Co_3Mo)$–fcc, κ-hcp and $\tau(Co_{0.818}Mo_{0.182}=Co_9Mo_2)$–fcc. Three isothermal sections were calculated, at 900, 1200 and 1500 K (Figs 4 to 6).

If we approximate the real system as a Co–30% Cr–5% Mo alloy, after a solution treatment at 1500 K, this composition lies on the border of the fcc/σ-fcc phase boundary (Fig. 6). One should note, however, that the cobalt-based surgical implant alloys also contain some nickel (Table I). Nickel, of course, is an autentitic stabilizer. Thus the effect of nickel on the phase diagram can be

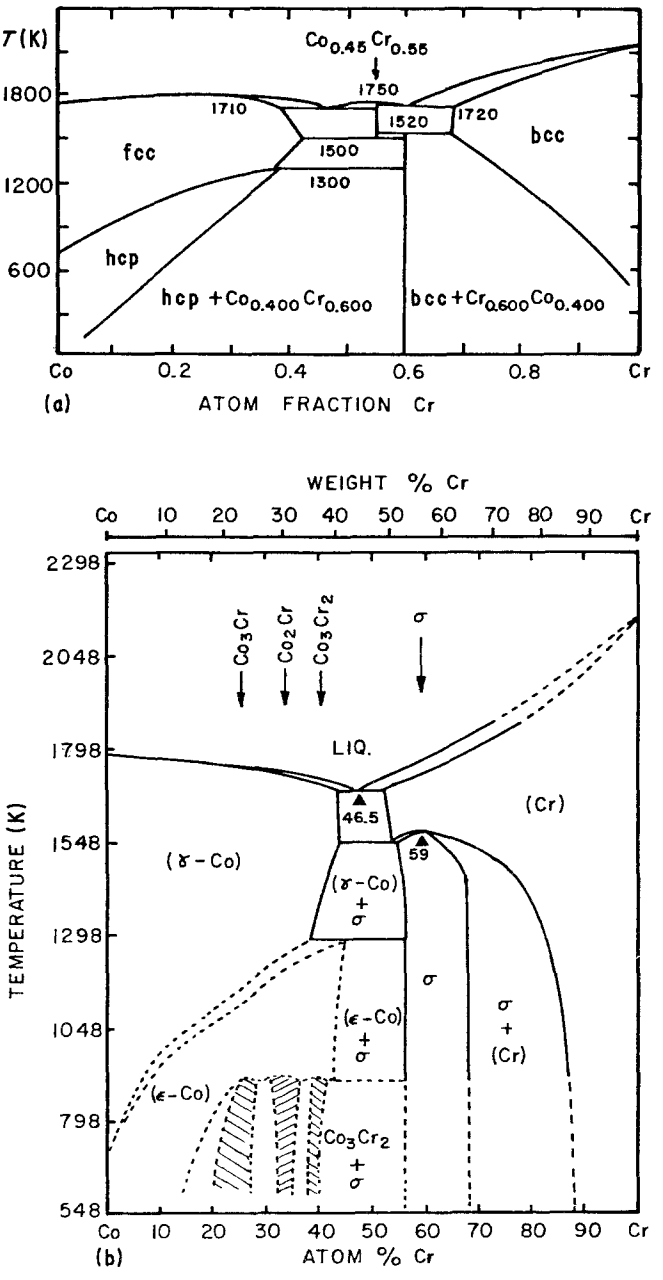

Figure 1 Comparison of (a) calculated and (b) experimental [5] Co–Cr phase diagrams.

qualitatively indicated by an enlarged fcc phase field. Thus the Co–30% Cr–5% Mo composition would now reside entirely in the fcc phase field after a heat treatment at 1500 K. However, if the alloy is given ageing treatments at lower temperatures that have been designed for carbide precipitation to aid in strengthening as suggested in the literature [1], the alloy composition is well within the σ + hcp phase field (Figs 5 and 6).

As a note of comparison, Rideout *et al.* [6] showed in 1951 an experimentally determined Co–Cr–Mo isotherm at 1200° C (~ 1500 K). It should be pointed out that the calculated isotherm of the present study was developed only for a limited composition range as discussed earlier. Also the ternary interaction parameter, Δ, was taken to be zero throughout the present calculations as mentioned previously. This could explain the absence of the ternary R-phase in the calculated diagram as compared to the experimental diagram of Rideout *et al.* However, the composition limits of the phase boundaries for the fcc, σ + fcc and μ + fcc regions do compare favourably between the 1951 article and the

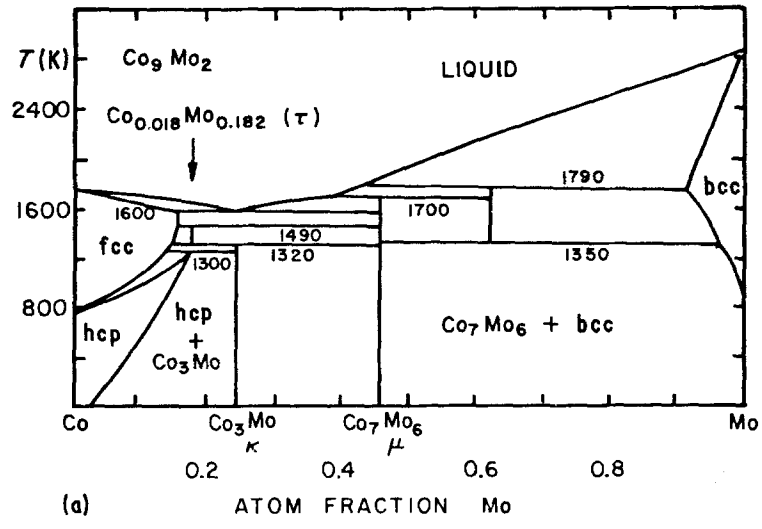

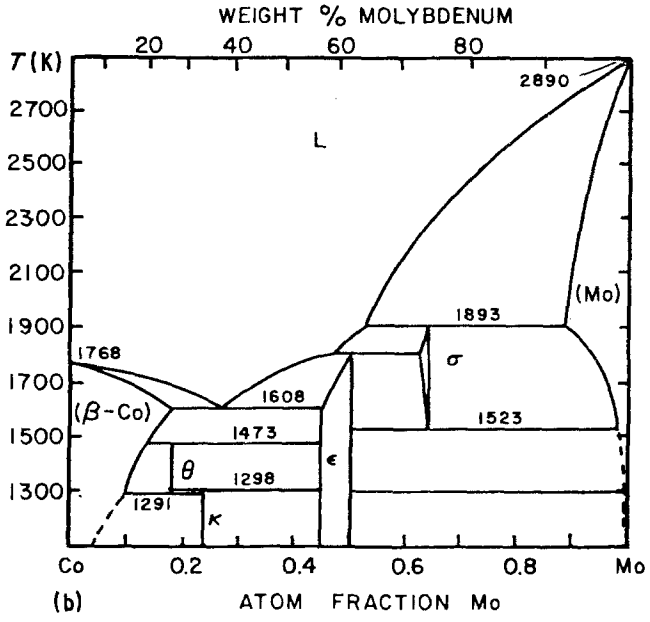

Figure 2 Comparison of (a) calculated and (b) experimental [4] Co–Mo phase diagrams.

present work. For example, along the Co–Mo binary, the fcc phase limit is at a Co/Mo atom ratio of 5.7 in the computed diagram while in the experimental diagram it occurs at a Co/Mo atom ratio of 5.4. Similarly, along the Co–Cr binary, the fcc limit in the computed diagram is at a Co/Cr ratio of 1.2 while in the experimental diagram this ratio is 1.6. In this study these are the areas of the phase diagram that are of primary interest.

3.2. Metallography

In this section we present metallography of samples given the heat treatment in which σ-phase is predicted to form. Also fractography of the

TABLE I Composition of as-cast alloy used in the present study

Elements	Composition (wt %)
Cr	28.5
Mo	5.7
Ni	2.2
Fe	0.4
C	0.3
Si	0.4
Mn	0.5
Co	Balance

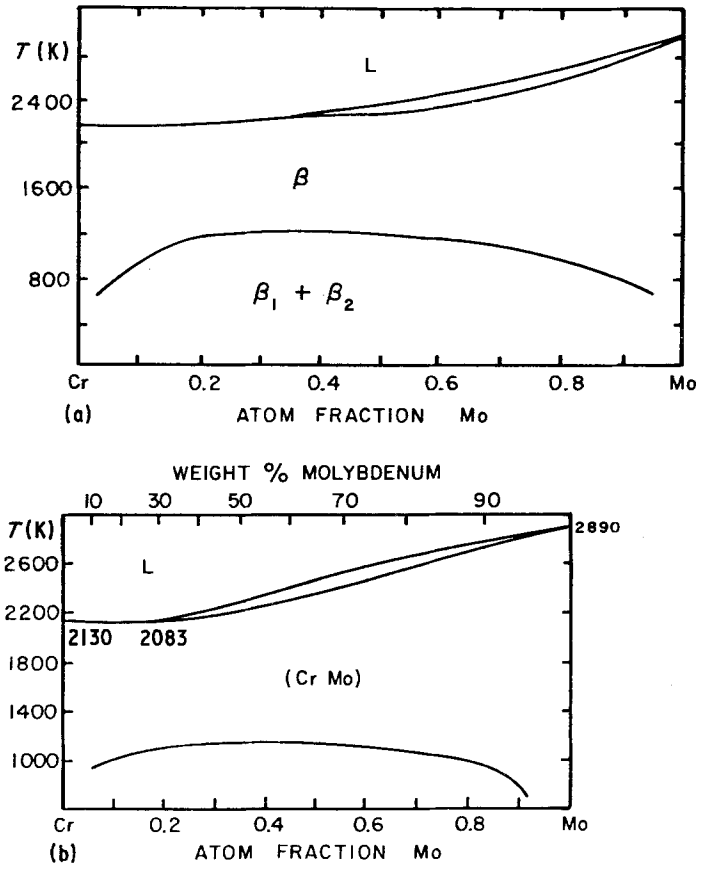

Figure 3 Comparison of (a) calculated and (b) experimental [4] Mo–Cr phase diagrams.

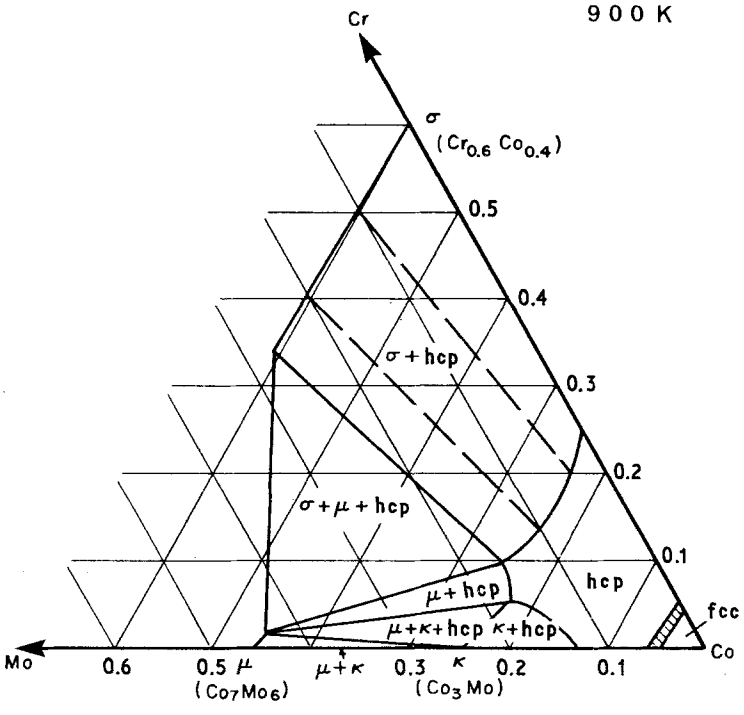

Figure 4 Computed Co–Cr–Mo phase diagram for 900 K.

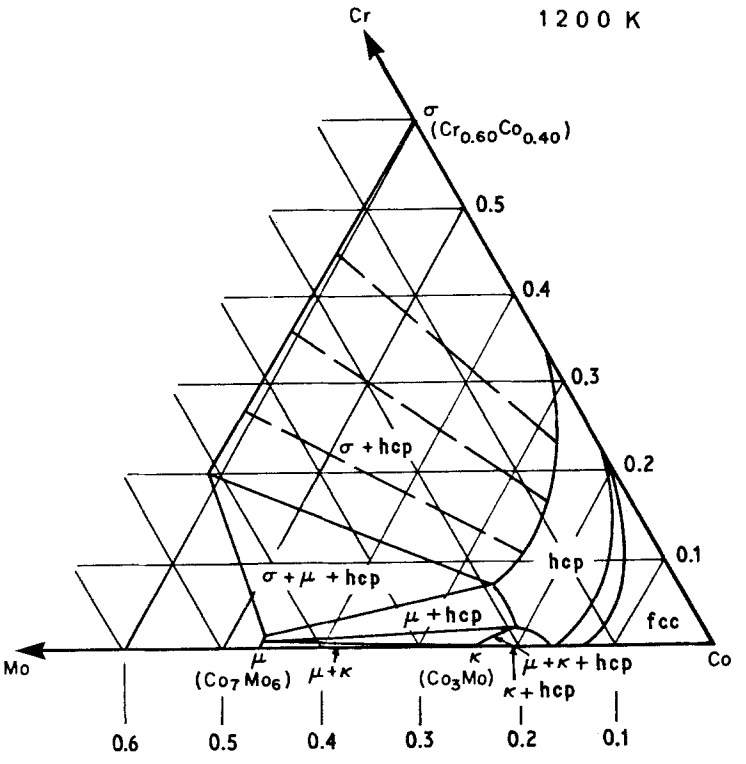

Figure 5 Computed Co–Cr–Mo phase diagram for 1200 K.

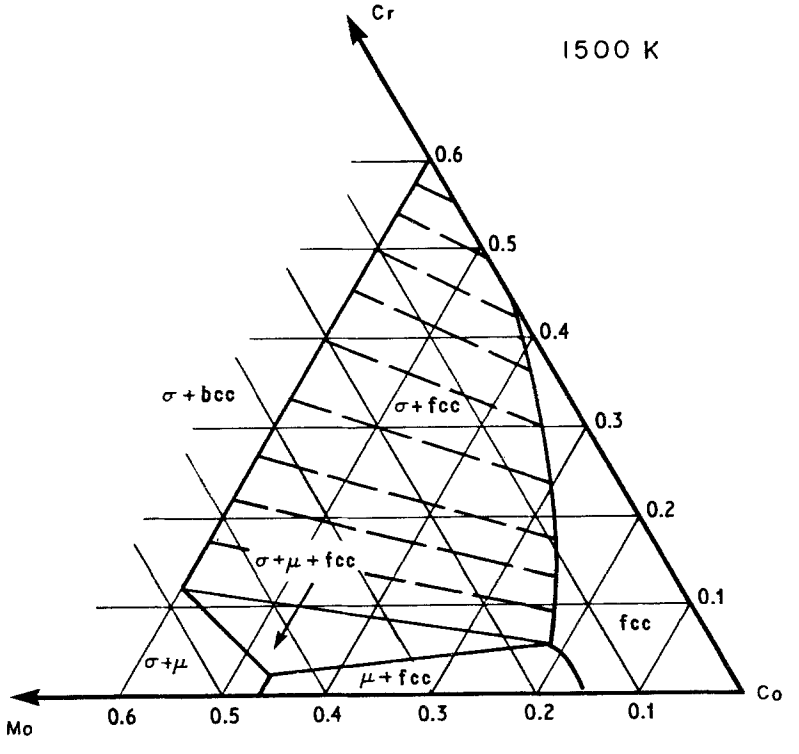

Figure 6 Computed Co–Cr–Mo phase diagram for 1500 K.

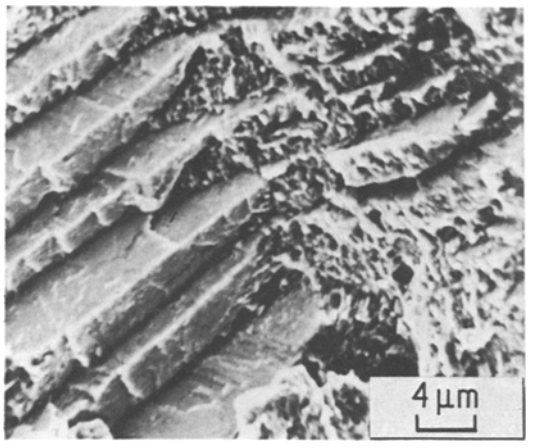

Figure 7 Transgranular region of fracture surface showing separation between matrix and plates (scanning electron micrograph).

tensile fracture surface of these samples is presented.

An examination of the fracture surface of a cast alloy aged for 30 h at 900 K showed that in regions of transgranular fracture, a dominant mechanism of fracture is separation between the matrix and a second phase which is in the form of plates (Fig. 7). A metallographic examination of the same fractured sample and a similarily heat-treated wrought HS 21 sample, showed plates of the same dimension ($\sim 2\,\mu$m thick) as those observed in the transgranular regions of the fracture surface (Figs. 8 and 9). The wrought microstructure exhibited a more profuse and homogeneous distribution of the plate-like second phase than the cast microstructure. However, in

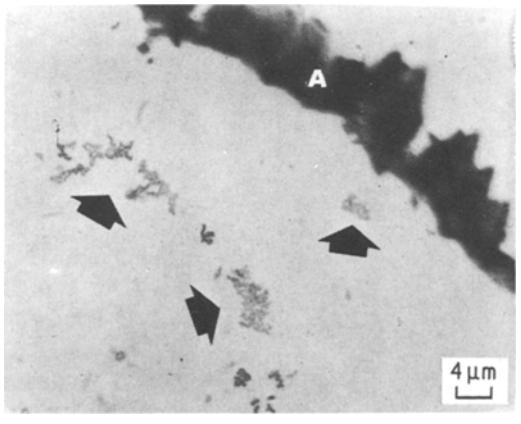

Figure 8 Metallographic cross-section of fracture sample shown in Fig. 7; showing grain-boundary carbides (A). Arrows indicate clusters of plates within the grain, probably σ-phase (optical micrograph).

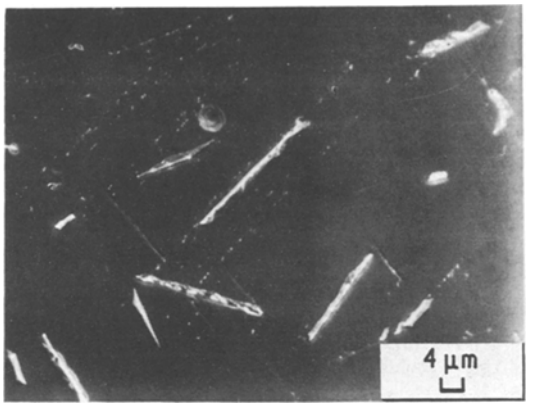

Figure 9 Wrought HS 21 of similar heat treatment to cast material, showing plate-like second phase within the grain, of similar dimensions to those on the fracture surface shown in Fig. 7 (scanning electron micrograph).

both cases, there is clearly evidence of a plate-like second phase in the grain interiors which matches the morphology and size of the plates in the transgranular regions of the fracture surface. These plates were also identified as sigma phase by their etching behaviour with Murakami's etchant [7].

Based on the appropriate isothermal section of the calculated ternary phase diagram, these plates are most probably σ-phase. For the alloy composition under consideration, the matrix should be hcp. However, as the kinetics of the fcc $\rightarrow$ hcp transition is very slow, the metastable fcc phase is retained [8]. The same cannot be said for σ-phase formation, and thermodynamically its formation is favoured at the ageing temperatures used.

4. Discussion

In previous work on this alloy system, Vander Sande *et al.* [1] attributed improvements in properties between processed and as-cast materials to the elimination of casting porosity. However, if one compares their limited mechanical property data of heat-treated cast and wrought materials separately, a different trend can be observed. Ageing a cast alloy at ~ 900 K for 20 h decreases its ductility as measured by the percentage elongation, to 17% from 21% in the solutionized state (~ 1500 K). A similar trend is observed for the wrought alloy with a drop in ductility of $\sim 22\%$ when the ageing time is increased from 2 h to 20 h.

While the elimination of casting porosity has long been established as being beneficial, the trend of decreasing ductility in both cast and

wrought materials upon certain heat treatments, suggests that another microstructural parameter must be considered. It is proposed here that this consistent loss in room-temperature ductility may be attributed to the development of the σ-phase as predicted by the calculated phase diagrams.

As pointed out earlier, fracture occurred by separation between the matrix and the second phase. This would suggest that the plates may act as crack-nucleation sites. The presence of a brittle plate-like phase such as σ would, therefore, not be desirable from the point of view of mechanical properties. Consequently, any benefit due to carbide precipitation from the ageing treatments could be negated.

While this paper has dealt with the prediction of intermetallic formation using computed phase diagrams of a ternary alloy, the role of carbon must not be ignored. After all, the real alloy system used in practice as surgical implant material is a Co–Cr–Mo–C system. However, owing to the limited amount of data on the Co–C system, the carbon interaction parameters were not available to be used in the calculations for this study. Nonetheless, from the information that is available, it has been shown by Krajewski *et al.* [9] and Koster [10] that carbon tends to enlarge the fcc phase field in cobalt. The stabilization of the fcc matrix implies an increase in the stacking fault energy (SFE) of the alloy. It has been shown previously by Rajan and Vander Sande [11] that the primary modes of strengthening in cobalt-based surgical implant alloys are fcc twinning and its structural precursor, stacking fault formation. Thus the effect of carbon on SFE can have an important effect on the work-hardening characteristics of the alloy. From this statement, one can easily draw the analogy to the effect of carbon on the work-hardening behaviour of metastable austenitic steels [12]. In that case, of course, carbon tends to lower the SFE of austenite rather than increase it as is the case with fcc cobalt. Lowering the SFE naturally allows for easier twin fomation and higher work-hardening rates.

While it is natural to view the role of carbon with respect to the formation of carbides [13], it is suggested here that its effect on the stabilization of the fcc phase (i.e. SFE) is just as an important effect to consider. This points out an area that needs a great deal of further experimental investigation.

5. Conclusion

The results of this study suggest some limitations with heat treatments used to promote carbide precipitation for strengthening. If these heat-treatment temperatures are to be considered, then there is the need for changes in alloy composition, since, as they are presently used, they do not suppress σ-phase formation. This demonstrates the need for a systematic analysis of the choice and amount of alloying elements to be added to the Co–Cr–Mo system for surgical implant applications. The use of calculated phase diagrams such as those presented here would help to provide a thermodynamic basis for alloy design.

References

1. J. B. VANDER SANDE, J. R. COKE and J. WULFF, *Met. Trans.* 7A (1976) 389.
2. L. KAUFMAN and H. BERNSTEIN, "Computer Calculation of Phase Diagrams" (Academic Press, New York, 1970).
3. L. KAUFMAN, "Report on the Proceedings of the Fourth Calphad Meeting" (NSF, NBS, Gaithersburg, Maryland, 1975).
4. R. HULTGREN, P. D. DESAI, D. T. HAWKINS, M. GLEISER and K. K. KELLEY, "Selected Values of the Thermodynamic Properties of Binary Alloys" (American Society for Metals, Metals Park, Ohio, 1973).
5. W. G. MOFFATT, "The Handbook of Binary Phase Diagrams" (General Electric Company, Schenectedy, New York, 1978).
6. S. RIDEOUT, W. D. MANLY, E. L. KAMEN, B. S. LEMENT and P. A. BECK, *Trans. AIME* **191** (1951) 872.
7. E. E. FLETCHER, Summary Report to the Office of Naval Research, Battelle Memorial Institute, 31 March, 1952 (Navy Department Contract no. N5 ori-111, Task Order 1, Project NR031-33).
8. K. RAJAN, *Met. Trans.* **13A** (1982) 1161.
9. W. KRAJEWSKI, J. KRUGER and H. WINTERHAGER, *Cobalt* **48** (1970) 120.
10. W. KOSTER, *Z. Metallk.* **43** (1952) 297.
11. K. RAJAN and J. B. VANDER SANDE, *J. Mater. Sci.* **17** (1982) 769.
12. R. W. K. HONEYCOMBE, "Steels – Microstructure and Properties" (Edward Arnold, London, 1981) p. 231.
13. W. KOSTER and F. SPERNER, *Arch. Eisenhittenw.* **26** (1955) 555.

Received 19 March
and accepted 2 July 1982